# What Factors Control the Size and Shape of Silver Nanoparticles in the Citrate Ion Reduction Method?

**Zeena S. Pillai and Prashant V. Kamat***

*Notre Dame Radiation Laboratory, Notre Dame, Indiana 46556-0579*

*Received: October 7, 2003*

Citrate ion, a commonly used reductant in metal colloid synthesis, undergoes strong surface interaction with silver nanocrystallites. The slow crystal growth observed as a result of the interaction between the silver surface and the citrate ion makes this reduction process unique compared to other chemical and radiolytic synthetic methods. Addition of citrate ions to preformed silver colloids (Ag-capped $SiO_2$) results in the complexation of citrate with silver colloids. The difference absorption spectra of $SiO_2$−Ag colloids in the presence of citrate ions show an increase in the absorption at 410 nm with increase in concentration of citrate. The apparent association constant as determined from these absorption changes is 220 $M^{-1}$. Pulse-radiolysis studies show that citrate ions complex with the silver seeds and influence the particle growth. For example, one of the primary intermediates, $Ag_2^+$ produced in the radiolytic reduction of silver ions, readily interacts with citrate to form a complex absorbing in the 410-nm region. The complex, [$Ag_2^+$−citrate], undergoes slower transformations compared to uncomplexed $Ag_2^+$. This slow transformation of the citrate complex eventually leads to the formation of larger clusters of silver. Steady-state and pulse-radiolysis experiments provide evidence for the multiple roles of citrate ions as a reductant, complexant, and stabilizer that collectively dictate the size and shape of silver nanocrystallites.

## Introduction

Metal particles in the nanometer size range have gained considerable interest in recent years as they serve as building blocks of next generation nanodevices.[1,2] Nanoparticles possess unique optical, electrical, and magnetic properties, which are strongly dependent on the size and shape of the particle.[3,4] They have potential applications in surface-enhanced Raman spectroscopy, display devices, catalysts, microelectronics (light-emitting diodes and photovoltaic cells), and as diagnostic biological probes.[4−17] Size provides important control over many of the physical and chemical properties of nanoscale materials including luminescence, conductivity, and catalytic activity.[18,19] Colloidal particles of varying size and shape have been synthesized using templates,[20−22] photochemistry,[23] seeds,[24−27] electrochemistry,[28−30] and radiolysis.[31−35]

The simplest and the most commonly used bulk-solution synthetic method for metal nanoparticles is the chemical reduction of metal salts. The particle synthesis usually makes use of a soluble metal salt, a reducing agent, and a stabilizing agent. The stabilizing agent caps the particle and prevents further growth or aggregation. Reducing agents such as sodium borohydride[36−39] and alcohols[40] are commonly used for the preparation of metal nanoparticles. Polymers and organic molecules bind to the particle surface and thus serve the role of a stabilizer. In the case of citrate reduction of gold and silver colloids, it serves the dual role of a reductant and a stabilizer. Since one can control the growth process by the choice of the stabilizer, it is possible to manipulate the shape and size of the metal nanoparticles.

Whereas citrate reduction produces nearly spherical Au nanoparticles, the same reduction procedure yields relatively large 60−200-nm diameter silver crystallites with a wide range of size and shape. In fact, these silver crystallites have proved to be the choice for surface-enhanced Raman spectroscopic measurements.[41−44] Moreover, the presence of citrate also facilitates photoconversion of silver nanospheres into triangular nanoprisms.[45] Despite the popular use of citrate for the reduction of silver ions, limited effort has been made to understand the exact role of the sodium citrate in controlling the shape of nanoparticles.[46] In the present work, we have investigated the early reduction steps using pulse radiolysis to understand the role of sodium citrate towards the growth of particles.

## Experimental Section

**Materials and Methods**. Sodium borohydride, silver nitrate, and silver perchlorate were obtained from Aldrich Chemical Co. and used as received. Sodium citrate was obtained from Alfa Aesar. $SiO_2$ (15 w/w %) colloids of particle diameter 50 Å, batch number B6M96, and suspended in an aqueous solution (pH 9.0) were obtained from Nalco Chemical Co. Deionized water was used for preparing aqueous solutions.

**Synthesis of Silver Nanoparticles.** Silver colloids were prepared by the well-known Turkevich method.[38] A solution of $AgNO_3$ ($\sim 1.0 \times 10^{-3}$ M) in deionized water was heated until it began to boil. Sodium citrate solution was added dropwise to the silver nitrate solution as soon as the boiling commenced. The color of the solution slowly turned into grayish yellow, indicating the reduction of the $Ag^+$ ions. Heating was continued for an additional 15 min, and then the solution was cooled to room temperature before employing for further experimentation.

**Ag-Capped $SiO_2$ Particles.** $AgNO_3$ (10 mL, $\sim 1.0 \times 10^{-3}$M) solution was added dropwise with stirring to a 10% $SiO_2$ (10 mL) suspension. Sodium borohydride solution in water was

* Author to whom correspondence may be addressed. E-mail: pkamat@nd.edu.

10.1021/jp037018r CCC: $27.50 
Published on Web 12/19/2003

added dropwise to the above mixture with stirring until the color changed to yellow. This method of preparation allowed us to stabilize the colloids without the addition of citrate.

**Transmission Electron Microscopy.** Transmission electron microscope (TEM) images were taken using a Hitachi H600 transmission electron microscope at a magnification factor of 200,000X. A drop of the suspension was placed on a carbon-coated grid for imaging and carefully blotted to remove excess water.

**Pulse Radiolysis.** Pulse-radiolysis experiments were performed using a model Titan Bet-8/16-1S LINAC. The linear accelerator produces electron pulses, 50 ns in duration, at an energy of 8 MeV. The dose in the pulse mode was determined to be approximately 6.13 Gy, based on the oxidation of thiocyanate ($SCN^-$) to $(SCN)_2^{\bullet -}$ in a $N_2O$-saturated solution. The solution flowed continuously through a quartz cell during the pulse-radiolysis experiment. Analysis of optical absorption vs time was done using ORIGIN (Microcal) software.

**$\gamma$ Radiolysis.** $\gamma$ radiolysis experiments were carried out in a Shepherd 109 cobalt-60 source, manufactured by the Shepherd Co. Cobalt-60 emits high-energy (1.25-MeV) photons. For reductive conditions, aqueous solutions were purged with $N_2$-(g) to saturate the solutions prior to $\gamma$ irradiation.

## Results and Discussion

**Reduction of Silver Ions Using Citrate Ions.** The Turkevich method[38] for preparing metal colloids employs sodium citrate, which serves the dual role of a reductant and stabilizer. Stable silver nanoparticles are formed when an aqueous solution of $AgNO_3$ (0.1−1.0 mM) is boiled in the presence of sodium citrate. The silver particles prepared by the citrate reduction method produce relatively large-sized (50−100-nm) silver crystallites with well-defined facets. Because of the wide dispersity of the particle size and shape, we observe broad surface plasmon absorption with a maximum around 420 nm. It should be noted that other reduction methods, using sodium borohydride[47] or radiolysis,[48] produce smaller-sized (5−20-nm diameter) spherical particles with sharp plasmon absorption in the 380−400-nm region. The difference in the absorption band and particle size of silver nanoparticles prepared using two different chemical reductants points out the unusual role of citrate ions in controlling the crystal growth and morphology of silver particles.

The reaction time for citrate reduction of $Ag^+$ ions at boiling temperature was found to be important for achieving complete reduction. For example, if we quickly cool the solution after boiling for 5−15 min, we obtain only partial reduction. The absorption spectra of the silver colloids obtained using different concentrations of citrate and boiling for 15 min are shown in Figure 1. Whereas most of the reduction is completed at a higher citrate concentration, only a small fraction of $Ag^+$ gets reduced at equimolar concentration. The overall spectral shape of the plasmon absorption remains the same, showing that the overall distribution of particles is unaffected by citrate concentration.

We followed the reduction of $Ag^+$ using sodium citrate by monitoring the absorption changes at different time intervals. The solutions were refluxed so that we did not lose any water by evaporation during boiling. Samples were withdrawn at different boiling times for recording absorption spectra. The absorption band at 420 nm grew as we continue the boiling process, showing increased reduction of $Ag^+$ ions. A plot of absorbance monitored at 420 nm vs reaction time is shown in Figure 2. When 1 mM sodium citrate was used, the absorbance value attained a plateau after 50 min whereas at higher

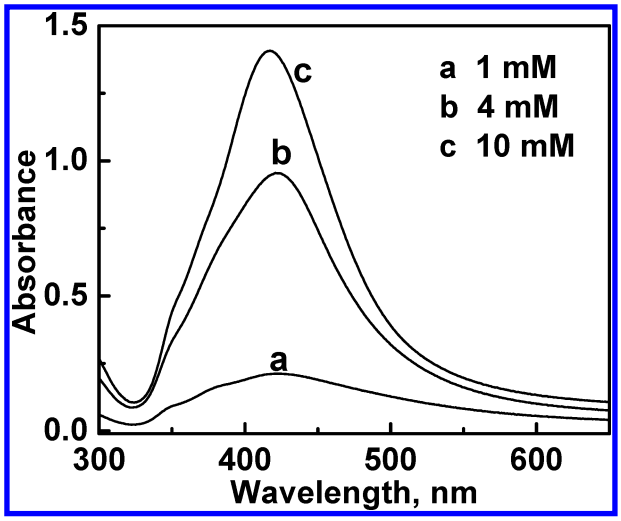


**Figure 1.** Absorption spectra of Ag colloids prepared using (a) 1mM, (b) 4mM, and (c) 10 mM of sodium citrate as the reductant. The boiling time was limited to 10 min. The concentration of $AgNO_3$ was 1 mM.

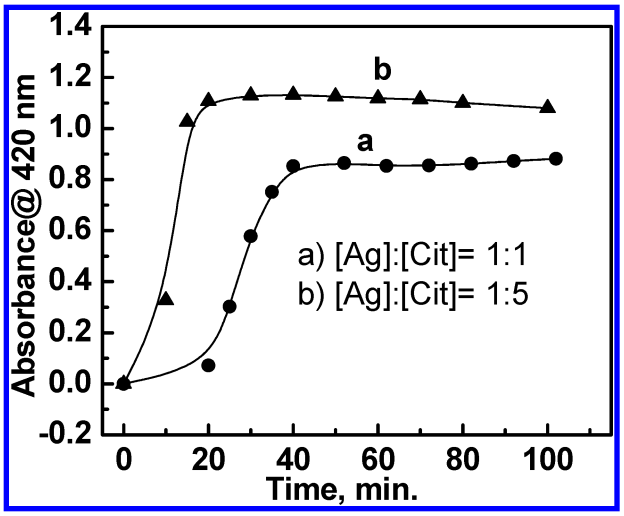


**Figure 2.** Plot of absorbance of Ag colloids at 420 nm at different reaction boiling times in the presence of 1 mM $AgNO_3$ and (a) 1 mM and (b) 5 mM of sodium citrate as the reductant.

concentration (5mM) of sodium citrate, the plateau was attained after 20 min. The observed increase in the plasmon absorbance at 420 nm with increasing citrate concentration indicates a greater amount of $Ag^+$ reduction. These observations show that sodium citrate brings about slow growth of silver particles and the reaction time is influenced by the concentration of sodium citrate. The decrease seen in the maximum absorbance (~20%) in trace a as compared to trace b in Figure 2 shows that a small fraction of the $Ag^+$ is likely to remain unreduced at low citrate concentrations.

In contrast, the silver colloids prepared by $\gamma$ radiolysis showed different absorption characteristics (Figure 3). A deaerated aqueous solution of $AgNO_3$ (1mM) containing different concentrations of sodium citrate was subjected to $\gamma$ irradiation. A small amount of methanol was added to scavenge hydroxyl radicals formed during the radiolysis.[46] The aqueous electrons formed during radiolysis initiate the reduction of $Ag^+$ ions (reaction 1) while the citrate ions present in the solution stabilize the colloidal suspension[46]

$$Ag^+ + e^-_{aq} \rightarrow Ag^0 \rightarrow\rightarrow (Ag)_n \qquad (1)$$

From the spectra presented in Figure 3, we find the absorption characteristics of Ag colloids to be independent of the citrate

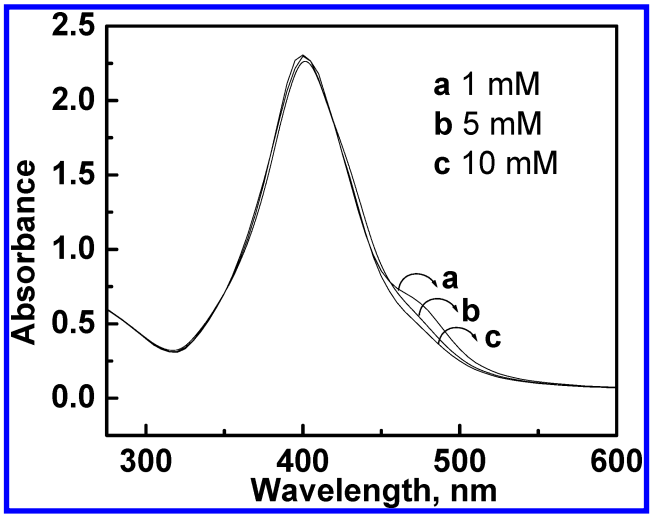


**Figure 3.** Absorption spectra of Ag colloids prepared by $\gamma$ irradiation of an aqueous solution ($N_2$ purged) containing 1 mM $AgNO_3$, 1% methanol, and (a) 1mM, (b) 5mM, and (c) 10 mM sodium citrate as stabilizer.

concentration and the absorbance maximum is maintained at 400 nm. Since the aqueous electron is a strong reductant, the $Ag^+$ ions are reduced quite effectively and quickly during radiolysis. As the silver seeds are continuously produced, the citrate stabilizer present in the solution arrests the colloid growth.

The difference in the absorption maximum of silver particles obtained using direct citrate reduction ($\lambda_{max}$ = 420 nm) and aqueous electrons ($\lambda_{max}$ = 400 nm) points out that the two reduction methods produce silver particles of different size and shape. It is interesting to note that in both of these reduction methods, the stabilizing species for silver colloids are citrate ions. However, the major difference between the two procedures is the nature of the reductant employed for the reduction of $Ag^+$ ions, i.e., the citrate ions are a milder reductant compared to the aqueous electrons.

**Transmission Electron Micrographs.** The morphology of silver nanoparticles was further established by recording transmission electron micrographs (TEM) of silver colloid suspension prepared by citrate reduction in the early (10 min) and final stage (2 h) of boiling (parts A and B, respectively, of Figure 4). TEM images of the silver particles at an earlier stage of growth (Figure 4A) showed small-sized spherical particles of diameter 3−5 nm, whereas the particles obtained after 2 h of boiling exhibit particles of diameter 40−60 nm (Figure 4B). Mostly large-sized Ag particles dominated the samples that were withdrawn at the end of reduction step, viz., after boiling the solution for 2 h. These observations show that smaller silver particles are formed in fewer numbers during the early stage of reduction, which then during the course of boiling grow to form large size crystallites.

The TEM image of the Ag colloids prepared by $\gamma$ radiolysis are shown in Figure 4C. The silver particles formed in the radiolytic reduction are nearly spherical and are 3−4 times smaller (15−20 nm) in diameter than those prepared by the citrate reduction method (particle diameter 50−100 nm). Obviously, continued formation of silver seeds during radiolysis results in smaller-sized particles. The differences in particle shape and size of silver particles formed in the citrate reduction and radiolysis experiments show that the mechanism of particle growth in these two reduction processes is different.

**Complexation between Preformed Silver Particles and Citrate Ions.** The surface complexation of metal nanoparticles with chemical species has been the topic of earlier investigations.[2,49−51] In our earlier study, we employed both NMR and absorption spectroscopy to probe the interaction of phenyl isothiocyanate and benzylamine with gold nanoparticles.[52,53] To probe the complexation of citrate with silver nanoparticles, we adopted another procedure that employed $SiO_2$ colloid as a stabilizer and $NaBH_4$ as a reductant.[53] This method allowed us to prepare silver nanoparticles in the absence of citrate ions. The absorption spectrum of $SiO_2$−Ag exhibits a sharp absorption band with a maximum at 380 nm (Figure 5, trace a). Upon addition of citrate to this solution, we observe a slight broadening of the band (Figure 5, trace b). The difference absorption spectra of the $SiO_2$@Ag colloids recorded at varying citrate concentrations are shown in Figure 6. With increasing concentration of sodium citrate, we observe an increase in the absorption at 410 nm. The presence of an isosbestic point observed with increasing citrate concentration confirms the existence of two species, viz., complexed and uncomplexed silver nanoparticles (equilibrium 2).

Such an interaction can be expressed in terms of equilibrium between $SiO_2$−Ag and citrate (equilibrium 2)

$$SiO_2-Ag + \text{citrate} \leftrightarrow (SiO_2-Ag-\text{citrate}) \qquad (2)$$

Since the maximum absorbance ($\Delta A_{max}$) at 410 nm is dependent on the concentration of the complex, one can employ the Benesi−Hildebrand method [54] to determine the apparent equilibrium constant. The inset of Figure 6 shows the dependence of $1/\Delta A$ on 1/[citrate]. From this plot, we obtain an apparent equilibrium constant of 220 $M^{-1}$ for the association between silver nanoparticles and sodium citrate. Such a high value of an apparent equilibrium constant suggests the strong affinity of sodium citrate to complex with silver colloids. Interaction of sodium citrate with silver colloids was further

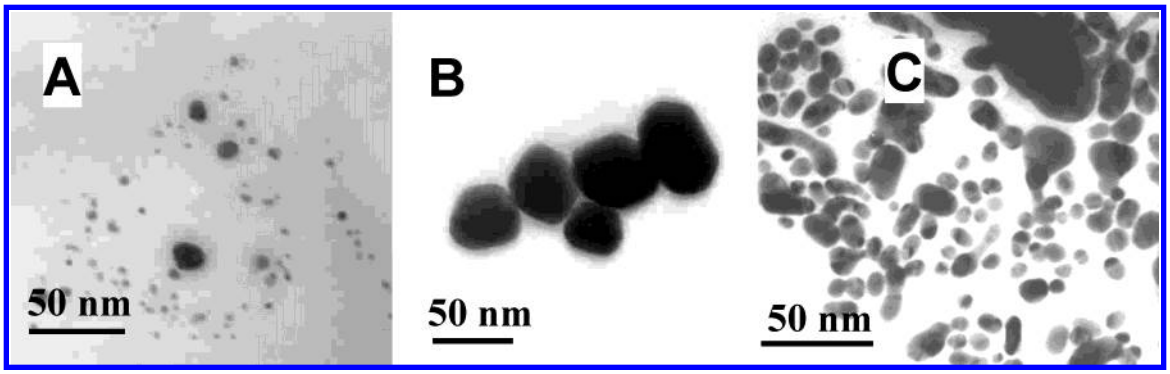


**Figure 4.** Transmission electron micrographs of silver colloid solution formed (A) at an earlier stage of reduction using sodium citrate as reductant, (B) at a later stage of reduction using sodium citrate as reductant, and (**C**) by $\gamma$ irradiation.

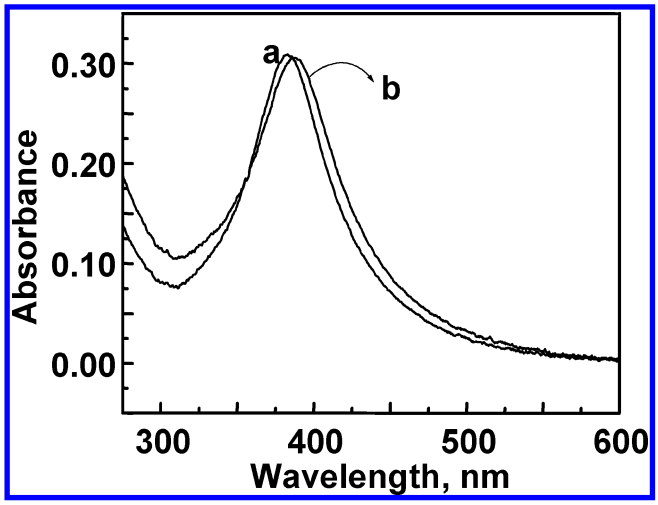


**Figure 5.** Absorption spectrum of (a) $SiO_2-Ag$ colloid (1 mM) and (b) $SiO_2-Ag$ colloid in the presence of sodium citrate (8.5 mM).

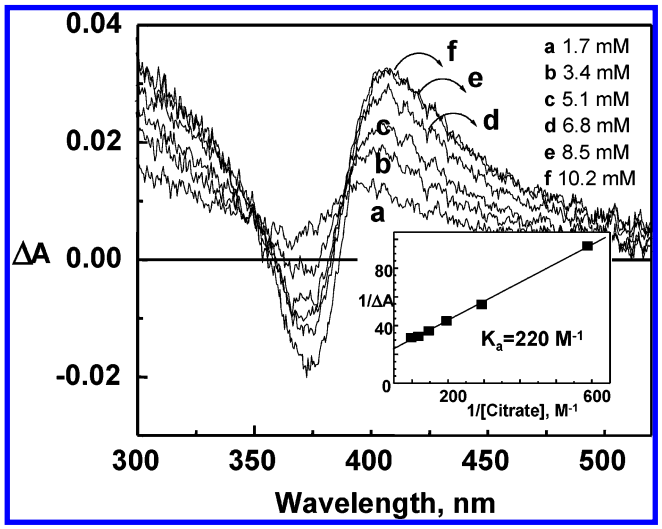


**Figure 6.** Difference absorption spectra of $SiO_2-Ag$ colloid (1 mM) in the presence of (a) 1.7 mM, (b) 3.4 mM, (c) 5.1 mM, (d) 6.8 mM, (e) 8.5 mM, and (f) 10.2 mM of sodium citrate. The inset shows the plot of $1/\Delta A_{max}$ (410 nm) vs 1/[sodium citrate].

probed using the pulse-radiolysis technique in order to obtain a better insight into the mechanistic aspects.

**Pulse Radiolytic Studies.** Pulse radiolysis was employed to probe the initial reduction of silver ions and primary growth steps involved in the formation of nanocrystallites. The primary products ($e_{aq}^-$, $OH^\bullet$, $H^\bullet$, etc.) formed during the radiolysis of water can be tuned to create controlled reductive or oxidative conditions. For example, we can achieve reductive conditions by adding *tert*-butyl alcohol (~2%) in a $N_2$ purged aqueous solution of $AgClO_4$. (*tert*-butyl alcohol is a good scavenger of hydroxyl radicals that are produced during radiolysis of water.) Thus, the aqueous electrons formed during radiolysis become the primary reductants as they react with $Ag^+$ ions.

The time-resolved difference absorption spectra recorded following the pulse radiolysis of an aqueous solution of silver perchlorate at different times are shown in Figure 7. The difference absorption spectrum recorded immediately after the electron pulse (trace a, Figure 7) shows a broad absorption in the region 300−450 nm, with a maximum at 360 nm, corresponding to the reduction of $Ag^+$ by aqueous electrons (reaction 3)

$$Ag^+ + e_{aq}^- \rightarrow Ag^0 \qquad (3)$$

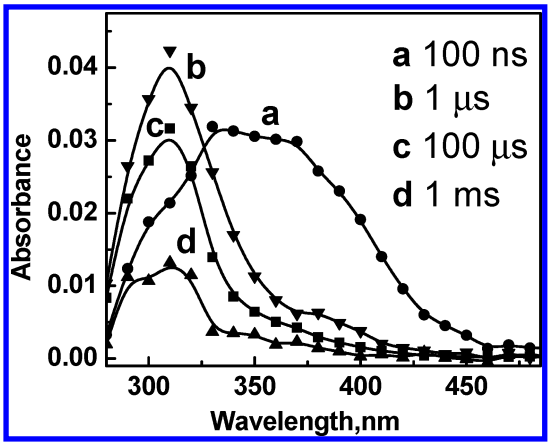


**Figure 7.** Transient absorption spectra recorded following the pulse radiolysis of $N_2$ saturated aqueous solution of silver perchlorate (1 mM) at (a) 100 ns, (b) 1 $\mu$s, (c) 100 $\mu$s, and d) 1 ms (~2% of *tert*-butyl alcohol was added as a scavenger for hydroxyl radicals).

As illustrated in an earlier study,[55] the absorption maximum at 360 nm is attributed to the formation of $Ag^0$. The absorption at 360 nm quickly decays over a period of ~0.3 $\mu$s, and a new absorption band at 310 nm appears (trace b, Figure 7). This new band at 310 nm is attributed to the absorption of $Ag_2^+$ (reaction 4)

$$Ag^0 + Ag^+ \rightarrow Ag_2^+ \qquad (4)$$

At longer times (1 ms), a new absorption band at 280 nm appears (seen as a shoulder in trace d, Figure 7) in correspondence with the decay of $Ag_2^+$. This absorption essentially arises from the dimerization of $Ag_2^+$ to form $Ag_4^{2+}$ (reaction 5)[55]

$$2Ag_2^+ \rightarrow Ag_4^{2+} \qquad (5)$$

The transient absorption spectra recorded following the pulse radiolysis of the aqueous solution of silver perchlorate in the presence of sodium citrate at different time scales are shown in Figure 8. The absorption maxima at short time scales (100 ns) are similar (spectra a and b in Figure 8A) to the one recorded in the absence of citrate. Although some broadening in the spectral profile is seen, the positions of the maxima are retained at 360 and 310 nm, respectively. These observations indicate that the first two primary reduction steps to form $Ag^0$ (reactions 3 and 4) are not significantly influenced by the presence of citrate ions.

However, a clear difference in the spectral profile is seen at a longer time scale (500 $\mu$s). A new broad absorption at 410 nm is seen in the presence of citrate. The transient decay profiles at 310 and 410 nm in the presence and absence of citrate are compared in parts A and B, respectively, of Figure 9. Following the decay at 310 nm, we observe a slower transient growth at 410 nm in the presence of sodium citrate. In the absence of citrate, the 310-nm transient decays within 2 ms, leaving more residual absorption. On the other hand, the trace recorded at 410 nm shows a slow absorption growth in the time scale of 8 ms. These observations suggest that the citrate anion is influencing the aggregation of $Ag_2^+$ (reaction 5) as it undergoes complexation with the positively charged silver dimer. Equilibrium 6 illustrates the formation of a complex between $(Ag_2)^+$ and citrate ion

$$(Ag)_2^+ + \text{citrate}^- \leftrightarrow [(Ag)_2^+ \cdots (\text{citrate})^-] \qquad (6)$$

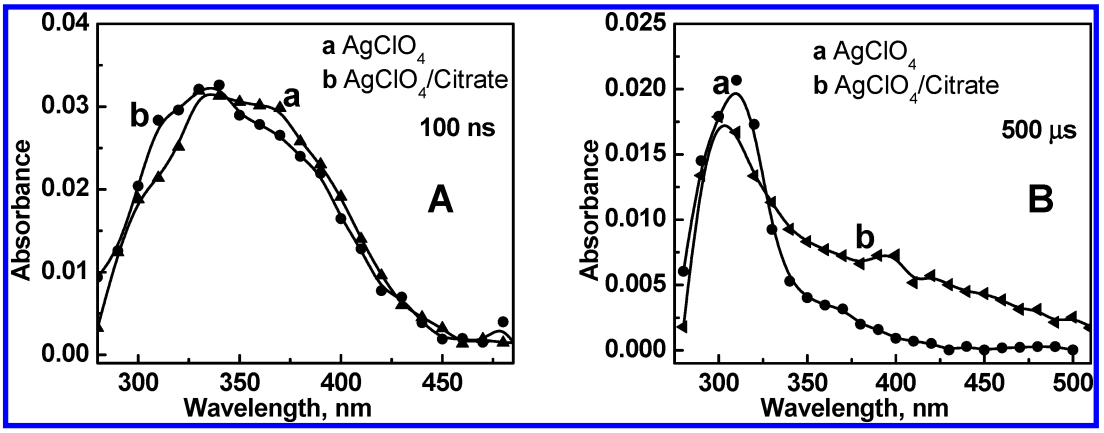


**Figure 8.** Transient absorption spectra recorded following the pulse radiolysis of $N_2$-saturated aqueous solution of silver perchlorate (~1 mM) in the presence and absence of sodium citrate at different times (A) 100 ns and (B) 500 $\mu$s (~2% of *tert*-butyl alcohol was added as a scavenger for hydroxyl radicals).

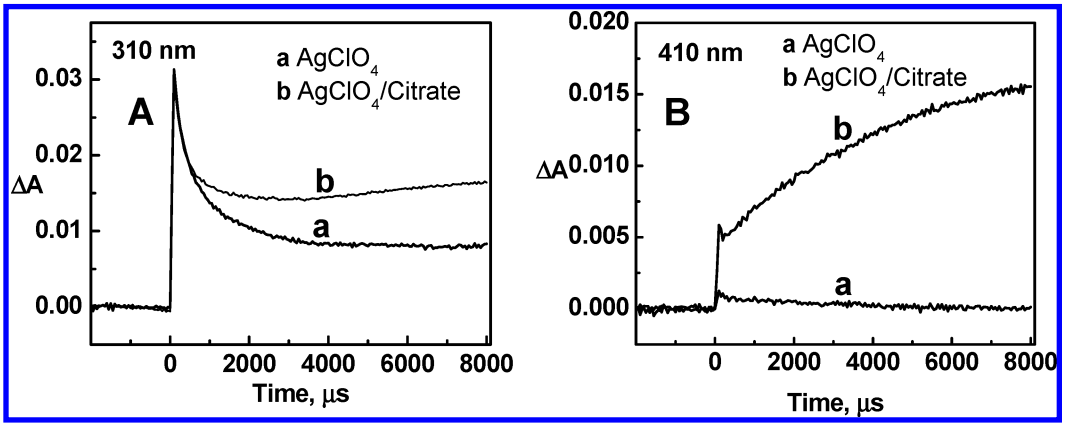


**Figure 9.** Transient-decay profiles recorded at (A) 310 nm and (B) 410 nm following the pulse radiolysis of $N_2$-saturated aqueous solution of 1 mM silver perchlorate (a) in the absence and (b) in the presence of sodium citrate (~5 mM). (~2% of *tert*-butyl alcohol was added as a scavenger for hydroxyl radicals.)

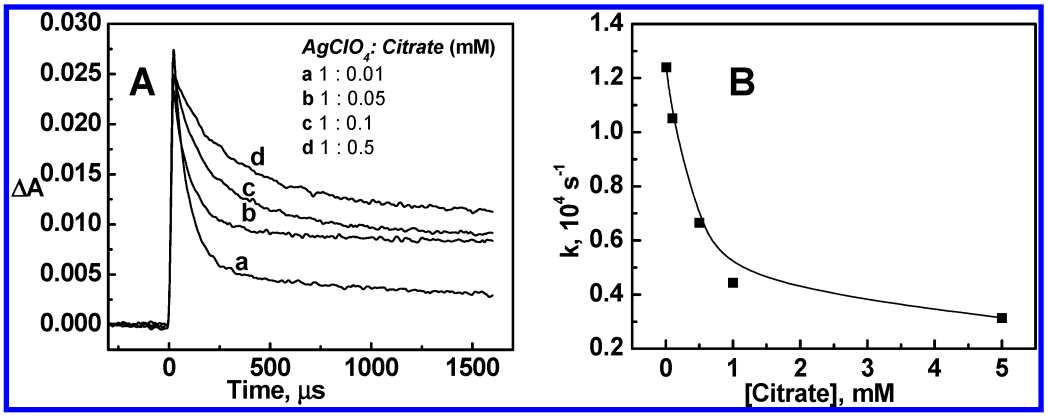


**Figure 10.** (A) Transient-decay profile at 310 nm following the pulse radiolysis of $N_2$-saturated aqueous solution of silver perchlorate (~1 mM) in the presence of (a) 0.01 mM, (b) 0.05 mM, (c) 0.1 mM, and (d) 0.5 mM sodium citrate (~2% of *t*-butanol was present to scavenge hydroxyl radicals). (B) Plot of decay rate constant at 310 nm vs the concentration of sodium citrate.

To further evaluate the complexation process, we monitored the transient decay at 310 nm (Figure 10) as well as the absorbance growth at 410 nm (Figure 11) at different concentrations of citrate. Citrate concentration was varied from 0.01−0.5 mM. The pseudo-first-order rate constant of the decay of the transient at 310 nm was found to decrease with an increase in concentration of sodium citrate (Figure 10B). In other words, the $Ag_2^+$ ions get stabilized as they complex with citrate ions and their conversion to $Ag_4^{2+}$ becomes slower. The lifetime of the $Ag_2^+$ ion increased from 80 to 320 $\mu$s as the concentration of sodium citrate was increased from 0.01 to 5 mM. Parallel to these changes, a transient growth at 410 nm was seen as we increase the concentrations of citrate (Figure 11A). The absorbance maximum of the transient at 410 nm plotted against concentration of citrate (Figure 11B) shows that the absorbance increases with increasing citrate concentration and attains a plateau at higher concentration of citrate ions. Obviously, at these high concentrations, we achieve complete complexation of the $Ag_2^+$ species with citrate ions.

During the radiolysis of aqueous solution, the silver seeds are produced by the reduction of metal ion precursors. These seeds agglomerate to form small silver clusters that further grow into larger clusters.[56,57] The presence of a stabilizer or complexing agent dictates the growth of these clusters.[35] Polymers

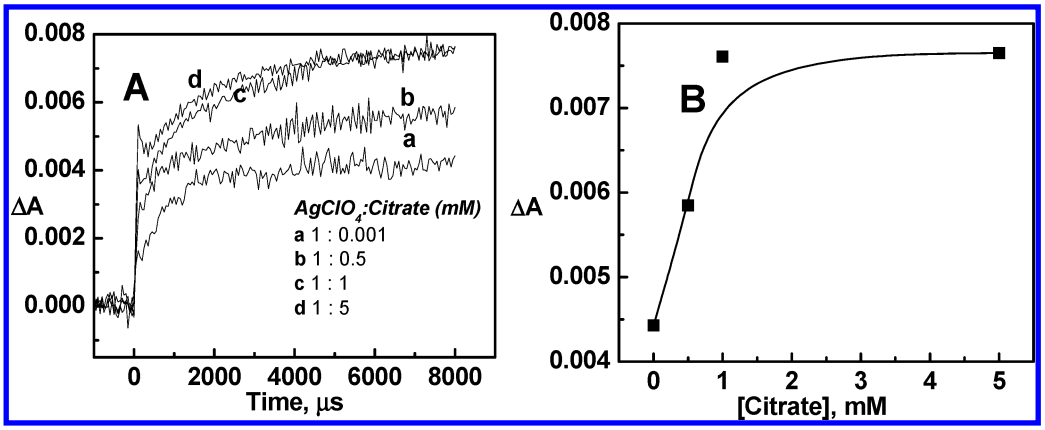


**Figure 11.** (A) Transient decay profile at 410 nm following the pulse radiolysis of $N_2$-saturated aqueous solution of silver perchlorate (~1 mM) in the presence of (a) 0.01 mM, (b) 0.5 mM, (c) 0.1 mM, and (d) 0.5 mM of sodium citrate. (B) Plot of maximum absorbance at 410 nm vs sodium citrate concentration.

**SCHEME 1. Primary and Secondary Growth Steps in the Formation of Silver Nanocrystallites**

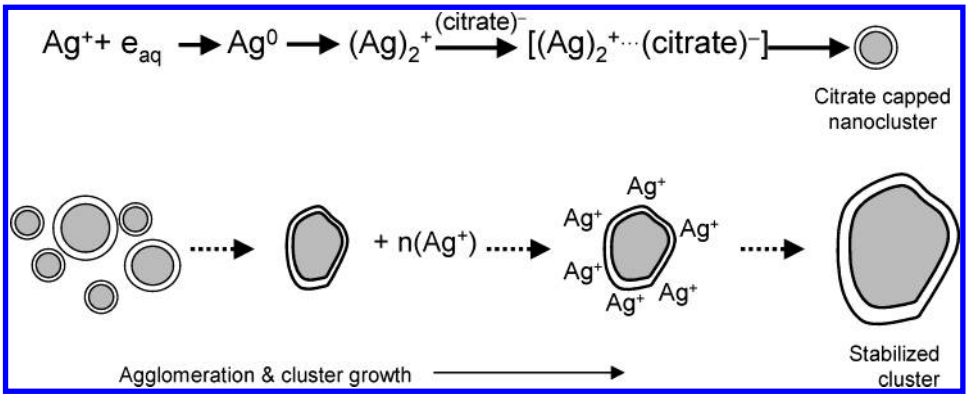


such as poly(vinyl alcohol), sodium dodecyl sulfate (SDS), sodium (polyvinyl sulfate) (PVS), and sodium polyacrylate (PA) have been used as stabilizers in the radiolytic preparation of metal clusters.[58−61] Covalent linkage or surface capping with an organic molecule at an early stage of cluster growth usually yields smaller-sized clusters. This strategy has been widely used to prepare size-selective semiconductor[62,63] and metal nanocrystallites.[64] Since citrate ions complex strongly at early growth stages, we would have expected to obtain smaller-sized silver clusters in the citrate reduction method. Instead, the citrate-induced chemical reduction produces larger clusters with various shape and size.

Henglein and Giersig[46] in a recent study of citrate capping of silver clusters have pointed out that at low concentrations of citrate ($1-5 \times 10^{-4}$ M) radiolytic reduction produces well-separated small spherical particles. On the other hand, at higher citrate concentration (>1.5 mM), they observed large-sized clusters with broad size distribution. They attributed this observation to the destabilization effect of citrate as it induces coalescence. In the citrate reduction procedure, initially few seeds of silver particles are formed, as is evident from the TEM image of silver colloids obtained at earlier stages of growth (Figure 4A). The seeds thus formed strongly complex with citrate anions. As the citrate complex slowly grows by further aggregation it reaches an optimal size at which stage the strong repelling layer of citrate prevents further aggregation. Further growth of these particles occurs via Ostwald ripening[65] in which larger particles grow at the expense of smaller ones. As the smaller particles are oxidized, the $Ag^+$ ions readsorb on the larger silver crystallites and undergo reduction at the metal surface. Such a reduction of $Ag^+$ ions at the silver surface is facilitated by the decrease in the reduction potential at the metal surface compared to the bulk solution. A detailed mechanism on the preferential reduction of metal ions at the preformed metal crystallites has been established in earlier studies.[66,67] The mechanism of citrate ion induced primary reduction step followed by the growth of silver nanocrystallites are illustrated in Scheme 1.

The complexation of citrate with silver surfaces discussed in the present study provides evidence for the slow particle growth observed in the citrate reduction process. As soon as silver seeds are formed in the initial reduction step, they complex with the citrate ions. As we loose the citrate from the bulk solution, we produce relatively fewer new seeds. With fewer initial silver seeds, we observe a growth of nanocrystals via Ostwald ripening as $Ag^+$ ions are reduced at the silver crystallite surface. Thus, greater reaction time (refluxing time) is needed to achieve almost complete reduction in a citrate reduction method.

## Conclusions

The complexation of citrate ions with silver plays an important role in dictating the size and shape of the silver nanocrystallites. As compared to the radiolytic reduction method, the citrate reduction produces larger crystallites. Steady-state measurements as well as pulse-radiolysis studies show that citrate ions have a high affinity for silver nanoparticles. Citrate ions influence the particle growth at early stages by complexing with positively charged $Ag_2^+$ dimers. Fewer seeds formed in the citrate reduction method and slow cluster growth contribute to the formation of larger silver nanocrystals of varying shape and size.

**Acknowledgment.** The work described herein was supported by the Office of Basic Energy Sciences of the U.S. Department

of Energy. This is contribution No. 4482 from the Notre Dame Radiation Laboratory. We would like to thank Drs. G. N. R. Tripathi and Dan Meisel for helpful discussions.

## References and Notes

(1) Adams, D.; Brus, L.; Chidsey, C. E. D.; Creager, S.; Cruetz, C.; Kagan, C. R.; Kamat, P. V.; Lieberman, M.; Lindsay, S.; Marcus, R. A.; Metzger, R. M.; Michel-Beyerle, M. E.; Miller, J. R.; Newton, M. D.; Rolison, D. R.; Sankey, O.; Schanze, K. S.; Yardley, J.; Zhu, X. *J. Phys. Chem. B* **2003**, *106*, 6668.

(2) Kamat, P. V. *J. Phys. Chem. B* **2002**, *106*, 7729.

(3) Creighton, J. A.; Eadon, D. G. *J. Chem. Soc., Faraday Trans.* **1991**, *87*, 3881.

(4) Cao, Y. W.; Jin, R.; Mirkin, C. A. *J. Am. Chem. Soc.* **2001**, *123*, 7961.

(5) Lee, P. C.; Meisel, D. *J. Catal.* **1981**, *70*, 160.

(6) Elghanian, R.; Storhoff, J. J.; Mucic, R. C.; Letsinger, R. L.; Mirkin, C. A. *Science* **1997**, *277*, 1078.

(7) Taton, T. A.; Mirkin, C. A.; Letsinger, R. L. *Science* **2000**, *289*, 1757.

(8) Chan, W. C. W.; Nie, S. M. *Science* **1998**, *281*, 2016.

(9) Cui, Y.; Wei, Q.; Park, H.; Lieber, C. M. *Science* **2001**, *2001*, 1289.

(10) Colvin, V. L.; Schlamp, M. C.; Alivisatos, A. P. *Nature* **1994**, *370*, 354.

(11) Klimov, V. I. *Science* **2000**, *290*, 314.

(12) Schatz, G. C.; Van Duyne, R. P. In *Handbook of Vibrational Spectroscopy*; Chalmers, J. M., Griffiths, P. R., Eds.; Wiley: New York, 2002; Vol. 1, p 759.

(13) Shim, M.; Guyot-Sionnest, P. *Nature* **2000**, *407*, 981.

(14) Beydoun, D.; Amal, R.; Low, G.; McEvoy, S. *J. Nanopart. Res.* **1999**, *1*, 439.

(15) Thurston, T. R.; Wilcoxin, J. P. *J. Phys. Chem. B* **1999**, *103*, 11.

(16) Mattousi, H.; Radzilowski, L. H.; Dabbousi, B. O.; Thomas, E. L.; Bawendi, M. G.; Rubner, M. F. *J. Appl. Phys.* **1998**, *83*, 7965.

(17) Hamilton, J. F.; Baetzold, R. C. *Science* **1979**, *205*, 1213.

(18) Alivisatos, A. P. *Science* **1996**, *271*, 933.

(19) Lieber, C. M. *Solid State Commun.* **1998**, *107*, 607.

(20) Foss, C. A.; Hornyak, G. L.; Stockert, J. A.; Martin, C. R. *J. Phys. Chem.* **1994**, *98*, 2963.

(21) Bohmer, M. R.; Fokkink, L. G. J.; Schonenberger, C.; van der Zande, B. M. I. *J. Phys. Chem. B* **1997**, *101*, 852.

(22) Nicewarner-Pena, S. R.; Freeman, R. G.; Reiss, B. D.; He, L.; Pena, D. J.; Walton, I. D.; Cromer, R.; Keating, C. D.; Natan, M. J. *Science* **2001**, *294*, 137.

(23) Esumi, K.; Matsuhisa, K.; Torigoe, K. *Langmuir* **1995**, *11*, 3285.

(24) Jana, N. R.; Gearheart, L.; Murphy, C. J. *Chem. Commun.* **2001**, 617.

(25) Jana, N. R.; Gearheart, L.; Murphy, C. J. *J. Phys. Chem. B* **2001**, *105*, 4065.

(26) Murphy, C. J.; Jana, N. R. *Adv. Mater.* **2002**, *14*, 80.

(27) Sun, Y. G.; Xia, Y. N. *Adv. Mater.* **2002**, *14*, 833.

(28) Yu, Y. Y.; Chang, S. S.; Lee, C. L.; Wang, C. R. C. *J. Phys. Chem. B* **1997**, *101*, 6661.

(29) Chang, S. S.; Shih, C. W.; Chen, C. D.; Lai, W. C.; Wang, C. R. C. *Langmuir* **1999**, *15*, 701.

(30) Nikoobhakt, B.; Wang, Z. L.; El-Sayed, M. A. *J. Phys. Chem. B* **2000**, *104*, 8635.

(31) Belloni, J.; Mostafavi, M.; Marignier, J. L.; Amblard, J. *J. Imaging Sci.* **1991**, *35*, 68.

(32) Belloni, J.; Amberland, J.; Delcourt, M. O. *Radiation Chemistry*; The Royal Society of Chemistry, 1994.

(33) Belloni, J. Photographic aspects of silver photography. In *Homogeneous Photocatalysis*; Chanon, M., Ed.; John Wiley & Sons, Ltd.: New York, 1997; p 170.

(34) Belloni, J. Photocatalytic aspects of silver photography. In *Homogeneous Photocatalysis*; Chanon, M., Ed.; John Wiley & Sons: New York, 1997; p 170.

(35) Belloni, J.; Mostafavi, M.; Remita, H.; Marignier, J. L.; Delcourt, M. O. *New J. Chem.* **1998**, *22*, 1239.

(36) Handley, D. A. *Colloidal Gold. Principles, Methods and Applications*; Academic Press: New York, 1989.

(37) Ahmadi, T. S.; Wang, Z. L.; Green, T. C.; Henglein, A.; El-Sayed, M. A. **1996**, *272*, 1924.

(38) Turkevich, J.; Stevenson, P. C.; Hiller, J. *Discuss. Faraday Soc.* **1951**, *11*, 55.

(39) Yee, C.; Scotti, M.; Ulman, A.; White, H.; Rafailovich, M.; Sokolov, J. *Langmuir* **1999**, *15*, 4314.

(40) Teranishi, T.; Hosoe, M.; Tanaka, T.; Miyake, M. *J. Phys. Chem.* **1999**, *103*, 3818.

(41) Lee, P. C.; Meisel, D. *J. Phys. Chem.* **1982**, *86*, 3391.

(42) Tripathi, G. N. R.; Clements, M. *J. Phys. Chem. B* **2003**, *107*, 11125.

(43) Schmid, G. *Chem. Rev.* **1992**, *92*, 1709.

(44) Sheng, R. S.; Zhu, L.; Morris, M. D. *Anal. Chem.* **1986**, *58*, 1116.

(45) Jin, R.; Cao, Y. W.; Mirkin, C. A.; Kelly, K. L.; Schatz, G. C.; Zheng, J. G. *Science* **2001**, *294*, 1901.

(46) Henglein, A.; Giersig, M. *J. Phys. Chem. B* **1999**, *103*, 9533.

(47) Nirmal, M.; Dabbousi, B. O.; Bawendi, M. G.; Macklin, J. J.; Trautman, J. K.; Harris, T. D.; Brus, L. E. *Nature* **1996**, *383*, 802.

(48) Henglein, A. *Langmuir* **1998**, *14*, 6738.

(49) Kreibig, U.; Gartz, M.; Hilger, A.; Hovel, H. Mie-plasmon spectroscopy: A tool of surface science. In *Fine Particles Science and Technology*; Pelizzatti, E., Ed.; Kulwer Academic Publishers: Boston, 1996; p 499.

(50) Linnert, T.; Mulvaney, P.; Henglein, A. *J. Phys. Chem.* **1993**, *97*, 679.

(51) Henglein, A.; Meisel, D. *J. Phys. Chem. B* **1998**, *102*, 8364.

(52) George Thomas, K.; Zajicek, J.; Kamat, P. V. *Langmuir* **2002**, *18*, 3722.

(53) Dawson, A.; Kamat, P. V. *J. Phys. Chem. B* **2000**, *104*, 11842.

(54) Benesi, H. A.; Hildebrand, J. H. *J. Am. Chem. Soc.* **1949**, *71*, 2703.

(55) Ershov, B. G.; Janata, E.; Henglein, A.; Fojtik, A. *J. Phys. Chem.* **1993**, *97*, 4589.

(56) Koulkes-Pujo, A. M.; Rashkov, S. *J. Chim. Phys.* **1967**, *64*, 534.

(57) Koulkes-Pujo, A. M.; Rashkov, S. *J. Chim. Phys.* **1968**, *65*, 911.

(58) Henglein, A. *J. Phys. Chem.* **1979**, *83*, 2209.

(59) Jonah, C. D.; Matheson, M. S.; Meisel, D. *J. Phys. Chem.* **1977**, *81*, 1805.

(60) Mostafavi, M.; Keghouche, N.; Delcourt, M.-O.; Belloni, J. *Chem. Phys. Lett.* **1990**, *167*, 193.

(61) Henglein, A. *Chem. Phys. Lett.* **1989**, *154*, 473.

(62) Herron, N.; Wang, Y.; Eckert, H. *J. Am. Chem. Soc.* **1990**, *112*, 1322.

(63) Bawendi, M. G.; Carroll, P. J.; Wilson, W. L.; Brus, L. E. *J. Chem. Phys.* **1992**, *96*, 946.

(64) Hostetler, M. J.; Wingate, J. E.; Zhong, C.-J.; Harris, J. E.; Vachet, R. W.; Clark, M. R.; Londono, J. D.; Green, S. J.; Stokes, J. J.; Wignall, G. D.; Glish, G. L.; Porter, M. D.; Evans, N. D.; Murray, R. W. *Langmuir* **1998**, *14*, 17.

(65) Hoang, T. K. N.; La, V. B.; Deriemeker, L.; Finsy, R. *Langmuir* **2002**, *18*, 10086.

(66) Meisel, D. *J. Am. Chem. Soc.* **1979**, *101*, 6133.

(67) Henglein, A.; Meisel, D. *Langmuir* **1998**, *14*, 7392.